Servo-elastic dynamics of a hydraulic actuator pitching a blade with large deflections

Hansen, Morten Hartvig; Kallesøe, Bjarne Skovmose

Published in:
Journal of Physics: Conference Series (Online)

Link to article, DOI:
10.1088/1742-6596/75/1/012077

Publication date:
2007

Document Version
Publisher's PDF, also known as Version of record

Servo-Elastic Dynamics of a Hydraulic Actuator Pitching a Blade with Large Deflections

2007 J. Phys.: Conf. Ser. 75 012077

(http://iopscience.iop.org/1742-6596/75/1/012077)

Journal of Physics: Conference Series **75** (2007) 012077 doi:10.1088/1742-6596/75/1/012077

Servo-Elastic Dynamics of a Hydraulic Actuator Pitching a Blade with Large Deflections

M. H. Hansen and B. S. Kallesøe

Wind Energy Department, Risø National Laboratory, Technical University of Denmark, DK-4000 Roskilde, Denmark

E-mail: morten.hansen@risoe.dk

Abstract. This paper deals with the servo-elastic dynamics of a hydraulic pitch actuator acting on a largely bend wind turbine blade. The compressibility of the oil and flexibility of the hoses introduce a dynamic mode in the pitch bearing degree of freedom. This mode may obtain negative damping if the proportional gain on the actuator position error is defined too large relative to the viscous forces in the hydraulic system and the total rotational inertia of the pitch bearing degree of freedom. A simple expression for the stability limit of this proportional gain is derived for tuning the gain based on the Ziegler-Nichols method. Computed transfer functions from reference to actual pitch angles indicate that the actuator can be approximated as a low-pass filter with some appropriate limitations on pitching speed and acceleration. The structural blade model includes the geometrical coupling of edgewise bending and torsion for large flapwise deflections. This coupling is shown to introduce edgewise bending response for pitch reference oscillations around the natural frequency of the edgewise bending mode, in which frequency range the transfer function from reference to actual pitch angle cannot be modeled as a simple low-pass filter. The pitch bearing is assumed to be frictionless as a first approximation.

1. Introduction

This paper deals with the modeling and analysis of the servo-elastic dynamics of a hydraulic pitch actuator acting on the blade of the 5 MW Reference Wind Turbine (RWT) by NREL [1]. This work has two objectives: A dynamic characterization of hydraulic pitch actuators and an identification of bending–torsion coupling effects for largely bend blades with pitch actuation.

The authors have not found any previous work on detailed modeling and analysis of hydraulic pitch actuators acting on wind turbine blades. Caselitz *et al.* [2] have presented a numerical–experimental analysis of a pitch controller using electrical pitch actuators, where the dynamics of these electrical actuators are included in the analysis as *hardware-in-the-loop*.

Nonlinear effects of large flapwise blade deflections on the power production and loads of MW-sized wind turbines have been studied from nonlinear aeroelastic simulations [3, 4]. These studies showed two main effects: A reduction in power production by up to 5 % due to reduced effective rotor area when the blade bend downwind and inward under the loading, and an increased pitch torque by up to 50 % at the blade root due to the increased distance from the pitch axis to the point of action of the inplane forces on the blade. The reduced power production is compensated by the controller through the blade pitch angle settings [3], which causes the blade loads and tower thrust loads to increase above rated wind speeds. The effect of the increased pitch torque on the pitch actuator and its control has not been considered.

These previous studies have focused on the mean steady effects of large blade deflections and less on the dynamic effects, except that it is mentioned that the frequencies of the edgewise modes are almost unchanged by the geometric coupling with torsion due to canceling inertia and stiffness effects [3]. The effects of large flapwise blade deflections on the aeroelastic stability characteristics of wind turbines were studied in the EU-funded STABCON project [5]. The edgewise bending–torsion coupling due to large flapwise blade deflection is shown to affect the aeroelastic damping of the first edgewise bending mode: The downwind bending of the blade during operation has a stabilizing effect on this damping; an effect that increases with decreasing torsional blade stiffness, showing that it is caused by the edgewise bending–torsion coupling.

A new aeroelastic blade model for wind turbine blades with pitch actuation [6] includes the bending–torsion coupling for largely bend blades and the inertia coupling from the rotational motion in the pitch bearing. A test case with the blade of the RWT shows that a step in the pitch angle induces both torsional and bending motion of the blade. The recent study using this aeroelastic blade model has shown that the flutter limit for the rotor speed of the RWT blade decreases with increasing flapwise downwind bending [7].

In this paper, the structural model of the RWT blade from [6] is coupled to a model of a hydraulic pitch actuator. The actuator is controlled by a proportional feedback of the piston position error to a proportional valve that regulates the flows to the two cylinder sides. The hydraulic model includes the compressibility of the oil and flexibility of the hoses, causing an actuator mode to arise in the characteristics of the actuator. The analysis of the blade-actuator dynamics shows that the transfer function from reference to actual pitch angles can be approximated below 10 Hz by a second order low-pass filter, except for frequencies around the natural frequencies of the edgewise bending and torsional blade modes and the actuator mode. The coupling to the edgewise bending mode only arises when the blade has a flapwise deflection.

2. Modeling of hydraulic pitch system

This section contains descriptions of the hydraulic pitch actuator model and the structural blade model. In this first approach to analyze the dynamics of a pitch system, gravity is neglected and only the static aerodynamic forces on the blade are included to obtain the right static blade deflection and static aerodynamic pitch torque.

2.1. Hydraulic pitch actuator model

Figure 1 shows the geometry and hydraulic circuit of the modeled pitch system. The actuator torque arm r_p, piston rod length l_p, and the pin–to–center length L determines the relationship between pitch angle θ_p and the position of the piston in the cylinder:

$$x_p(\theta_p) = \sqrt{L^2 + r_p^2 - 2Lr_p\cos(\alpha_0 + \theta_p)} - l_p \tag{1}$$

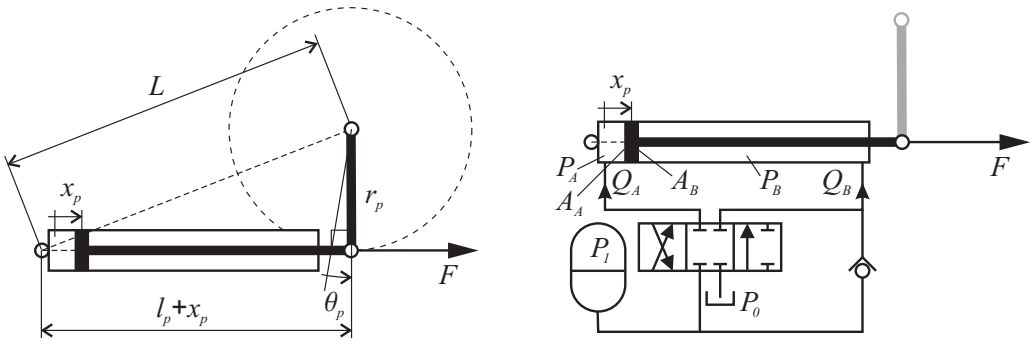

Figure 1. Geometry (left) and hydraulic circuit (right) of the modeled pitch system.

with $x_p = 0$ at the minimum pitch angle. The piston force F creates a pitch torque:

$$T_p = F r_p g(\theta_p) \tag{2}$$

where the function $g(\theta_p)$ is a force factor given by $g(\theta_p) = \frac{1}{r_p}\frac{dx_p}{d\theta_p}$. The piston rod length l_p and the torque arm r_p are chosen to be 2 m and 1 m, respectively, for the pitch actuator developed for the RWT. The minimum pitch angle is -5 deg and the distance $L = 2.3$ m is chosen such that the maximum force factor $g = 1$ occurs at zero pitch angle $\theta_p = 0$, where it is assumed that the maximum torque is required. Note that these geometric parameters are arbitrarily chosen, but realistic values; in an actual design of the actuator they are part of the optimization process.

Figure 2 shows the cylinder position and force factor as function of the pitch angle in the range -5 to 90 deg. In the normal operating range 0 – 23 deg, the force factor is not lower than 0.93 and the piston position depends almost linearily on the pitch angle.

The diagram of the hydraulic circuit in Figure 1 shows that the pitch actuator is driven by an accumulator with an assumed constant pressure $P_1 = 250$ bar. The pressures in the cylinder are denoted P_A on the left side (A-side) of the piston and P_B on the right side (B-side) of the piston, where the area A_B (piston rod diameter 0.115 m) is smaller than the area A_A (bore diameter 0.2 m) on the left side. The piston force therefore becomes:

$$F = P_A A_A - P_B A_B - \eta \dot{x}_p \tag{3}$$

where $\dot{(\cdot)} = \frac{d}{dt}$ denotes the time derivative, and the last term models the viscous damping force on the moving piston given by the coefficient η. The flows Q_A and Q_B to the two cylinder sides are governed by a proportional valve which is controlled by a piston position error feedback as

$$u = k_p \left(x_p(\theta_p) - x_p(\theta_{ref}) \right) \tag{4}$$

where u is the control voltage to the valve, k_p is the proportional gain, and the position error is given as function of the actual and reference pitch angles θ_p and θ_{ref}, respectively.

A valve flow is assumed to be proportional to the square-root of the pressure difference over the valve $Q = K\sqrt{\Delta P}$, where K is a flow constant depending on the control voltage. Figure 3 shows in the top plot the flow constants as function of the control voltage u for the flows through the proportional valve. The maximum flow constants at $|u| > 10$ V for flows to and from the A-side of the cylinder are 200 l/min/bar$^{\frac{1}{2}}$, and 100 l/min/bar$^{\frac{1}{2}}$ for a flow to the B-side of the cylinder. There is a deadzone for control voltages around zero $|u| < 1$ V, where the valve moves from one side to the other. This deadzone can be compensated by modulation of the control voltage, which in this first study is assumed to be ideal as shown in the bottom plot of Figure 3.

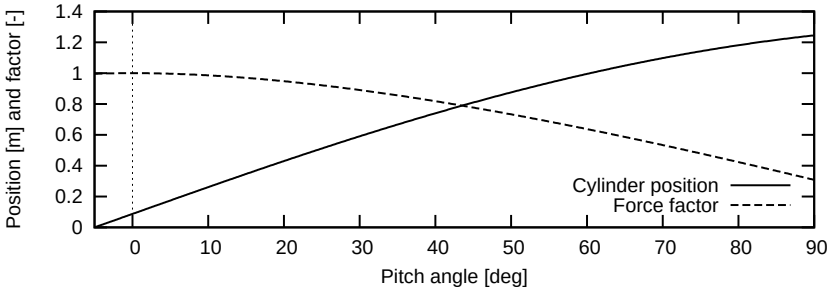

Figure 2. Plots of the geometrical relationships between pitch angle and the cylinder position and the geometrical force factor of piston force to actuator torque.

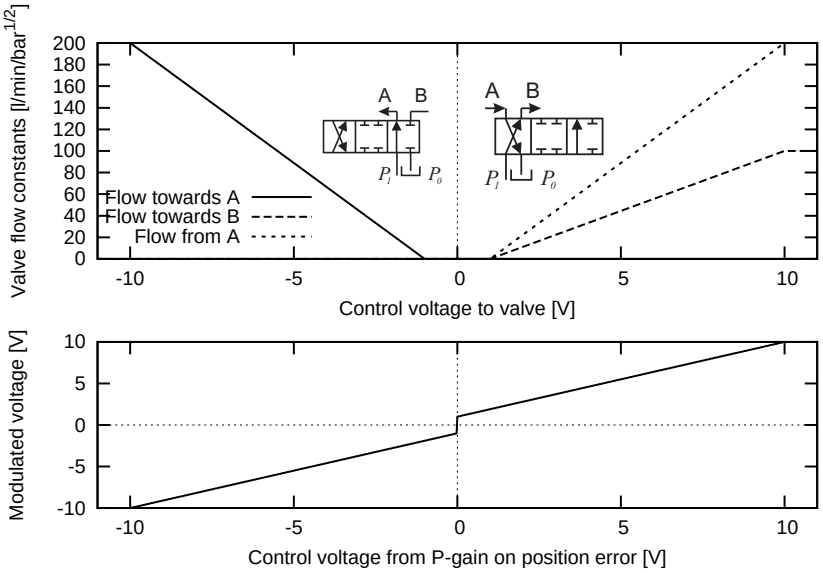

Figure 3. Flow constants as function of control voltage to the proportional valve including a deadzone around zero (top plot), which is assumed to be ideally compensated by the modulation of the control voltage as shown in the bottom plot.

For $u > 1$, the valve is in its left position, where oil can flow from the accumulator into the B-side, and out of the A-side into the sump. The pressure differences over the valve for the A- and B-sides are $P_A - P_0$ and $P_1 - P_B$, respectively.

For $u < -1$, the valve is in its right position, where oil can flow from the accumulator into the A-side and out of B-side back into the accumulator through the check valve if the pressure is (slightly) larger than the accumulator pressure $P_B > P_1$. The pressure difference over the proportional valve for the A-side is $P_1 - P_A$, and it is $P_B - P_1$ over the check valve for B-side.

The flow constant for the check valve is 50 l/min/bar$^{\frac{1}{2}}$, which is obtained for a pressure difference $P_B - P_1$ of more than 4 bars to model a spring-like behavior of the check valve opening. Finally, flow limits of 300 l/min and 50 l/min on the maximum obtainable flows in the proportional valve and the check valve, respectively, are imposed. Note again that these valve parameters are arbitrarily chosen, but realistic values; in an actual actuator design, the choices of valves are also part of the optimization process.

The compressibility of the hydraulic oil and the flexibility of the hoses are modeled by an effective bulk modulus β of 7000 bars for the system of oil and hoses yielding

$$\beta = \rho \frac{dp}{d\rho} \Rightarrow dp = \frac{\beta}{\rho} d\rho = \frac{\beta}{V} \left(\frac{dm}{\rho} - dV \right) \tag{5}$$

A variation in pressure dp can arise from variation in mass dm and in volume dV. The flow Q to a volume V represents a variation in mass of $dm = \rho Q dt$. Using the effective bulk modulus and this relation, the time derivatives of the pressures in cylinder become:

$$\dot{P}_A = \frac{\beta}{V_A(x_p)} \left(Q_A(P_A, u) - \dot{x}_p A_A \right) \quad \text{and} \quad \dot{P}_B = \frac{\beta}{V_B(x_p)} \left(Q_B(P_B, u) + \dot{x}_p A_B \right) \tag{6}$$

where $V_A(x_p)$ and $V_B(x_p)$ are the volumes on A- and B-sides of the piston as function of the piston position. These volume functions include the hose-volumes and "unusable" cylinder volumes, which are assumed to be $V_A(0) = V_B(l_p) = 5$ l.

2.2. Structural blade model
The structural blade model is based on the model by Kallesøe [6] using second order Bernoulli-Euler beam theory. The model of the RWT blade is identical to the linear model used in [6] with three assumed blade modes in a modal expansion: The first flapwise and edgewise bending modes and a first torsional mode. The pitch bearing degree of freedom is included in the model with inertia coupling terms to all three assumed blade modes, which are strongest for the torsional mode and the edgewise bending mode when the blade is bend flapwise. Figure 4 illustrates the sign of the four degrees of freedom.

The linear equations of blade motion are:

$$\mathbf{M}\ddot{\mathbf{q}} + (\mathbf{G} + \mathbf{C})\,\dot{\mathbf{q}} + \mathbf{K}\mathbf{q} = \mathbf{F}\,(T_p + T_0) \tag{7}$$

where the vector $\mathbf{q} = \{q_e, q_f, q_t, \theta_p\}^T$ contains the four generalized coordinates for edgewise, flapwise, torsional and pitching motions of the blade, T_0 is the steady state aerodynamic torque, and $\mathbf{F}$ is the single column matrix $\mathbf{F}^T = [0, 0, 0, 1]$. Matrices $\mathbf{M}$, $\mathbf{G}$, $\mathbf{C}$, and $\mathbf{K}$ are mass, gyroscopic, damping and stiffness matrices, which (except the damping matrix) depend on deformation state of the blade. Linear models for the undeformed (unloaded) and deformed blade (loaded as under operation at 12 m/s) are computed. The damping matrix $\mathbf{C}$ is computed as Spectral Damping [8], where the two bending modes and the torsional mode are set to have logarithmic decrements of 2 % and 4 %, respectively.

Note that the unsteady aerodynamic blade forces are neglected in the blade model; only the steady state aerodynamic pitch torque is used in the analysis to obtain the right mean hydraulic pressures. Frictional torque in the pitch bearing is also neglected in this first approach analysis of pitch bearing-blade-actuator dynamics.

3. Stability limit for the proportional gain

This section contains a stability analysis of the hydraulic pitch actuator assuming that the deformed blade is rigid with a moment of inertia about the pitch axis of I_p. The following assumptions are furthermore made to enable the linearization of the hydraulic system:

- Mean actual and reference pitch angles are zero $\bar{\theta}_p = \bar{\theta}_{ref} = 0$ deg, whereby $dg/d\theta_p = 0$
- Variation of the actual pitch angle is small $\delta\theta_p << 1$
- Mean A-side pressure is the averaged of accumulator and sump pressures $\bar{P}_A = (P_0 + P_1)/2$
- Variation of the A-side pressure is small $\delta P_A << 1$
- B-side pressure is the accumulator pressure $P_B = P_1$ and constant $\delta P_B = 0$

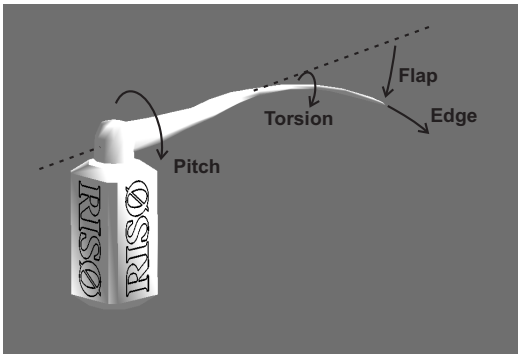

Figure 4. Illustration of the degrees of freedom in the blade model with three selected assumed modes: Flapwise and edgewise bending and torsional modes.

With these assumptions, the linear governing equations for the small variations of pitch angle and A-side pressure can be written as

$$\dot{\mathbf{y}} = \mathbf{A}\mathbf{y} \quad , \text{where} \quad \mathbf{A} = \begin{bmatrix} 0 & 1 & 0 \\ 0 & -\frac{\eta r_p^2}{I_p} & \frac{A_A r_p}{I_p} \\ -c_1 k_p & -c_2 & 0 \end{bmatrix} \tag{8}$$

where the state vector $\mathbf{y} = \{\delta\theta_p, \delta\dot{\theta}_p, \delta P_A\}^T$ contains the variations, and the constants c_1 and c_2 are given by the A-side valve flow constant (cf. Figure 3), the averaged pressure differential $(P_1 - P_0)/2$, the bulk modulus β, and the geometrical parameters r_p, l_p, and L.

Using the Routh-Hurwitz criteria for negative real parts of all eigenvalues of $\mathbf{A}$, which ensures that any disturbance of the pitch angle away from its equilibrium is damped, the following expression for the stability limit on the gain can be derived:

$$k_{p,crit} = \frac{\eta r_p^2}{I_p} \frac{A_A}{K_{A,u}\sqrt{(P_1 - P_0)/2}} \tag{9}$$

where $K_{A,u}$ is the slope of the linear flow constant function of the control voltage u for the A-side of the proportional valve with ideal deadzone compensation.

This critical gain shows that the viscous damping in the pitch system given by the coefficient η has a stabilizing effect, whereas the normalized rotational pitch inertia I_p/r_p^2 has a destabilizing effect in the position error feedback loop of the actuator. The inverse of the term $A_A/(K_{A,u}\sqrt{(P_1 - P_0)/2})$ is the area normalized gradient of the flow over the proportional valve with respect to the control voltage. This term shows destabilizing effects of the proportional valve size given by $K_{A,u}$ and the pressure differential over the valve given by $(P1 - P0)/2$, which can be compensated by a larger cylinder bore area A_A.

For sub-critical gains $k_p < k_{p,crit}$, the actual pitch angle will return to the reference pitch angle after a disturbance; however, too low a gain leads to a long return period, whereas a gain close to the critical gain leads to low damped oscillations of the pitch angle. Using the Ziegler-Nichols method, the gain is therefore set to half of the critical value $k_p = k_{p,crit}/2$.

Figure 5 shows the natural frequency and damping in terms of the real part of the eigenvalue of the feedback mode in the linearized pitch system. The natural frequency of this mode is around 7 Hz and the damping becomes negative (positive real part of the eigenvalue) around 90 V/m, which agrees with a derived critical gain. The gain is therefore set to 45 V/m in the following analysis including the blade flexibility.

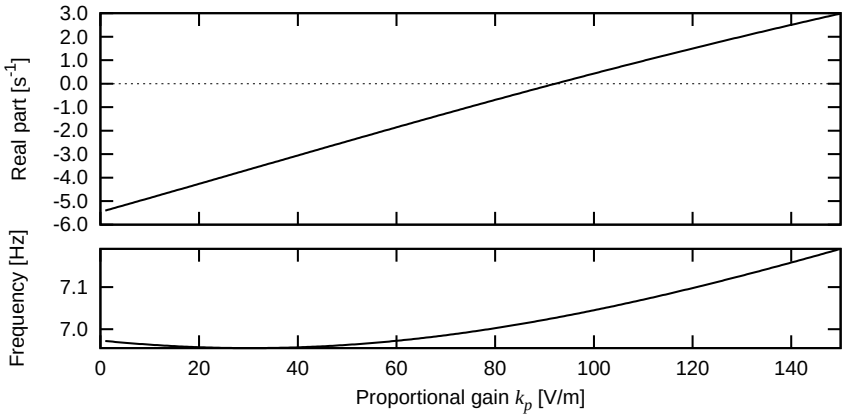

Figure 5. Natural frequency and real part of eigenvalue (damping) of feedback mode in the hydraulic pitch actuator as function of the gain k_p.

4. Transfer function from reference to actual pitch

This section contains computations of the transfer function from reference to actual pitch angle based on the model of the hydraulic actuator. A complex transfer function $H(\omega)$ from reference to actual pitch angles describes the actual pitch angle response to excitation with a harmonic pitch reference variation $\theta_{ref} = a \sin \omega t$. For a given amplitude a and frequency ω, the actual pitch angle response is assumed to be given by $\theta_p = a|H(\omega)| \sin(\omega t + \arg(H(\omega)))$. This linear approximation assumes that actual pitch angle response contains only one harmonic with the frequency ω. The strong nonlinear dynamics of the actuator may lead to off-frequency contents in the response; however, in the present analysis significant off-frequency responses are only seen in the blade modal responses and not in the pitch response.

The computation of the linear transfer functions from the nonlinear model given by the hydraulic actuator model (6) and structural model (7) is based on the Finite-Difference Method for construction of periodic solutions in nonlinear dynamic systems [9]. The harmonic pitch reference variation $\theta_{ref} = a \sin \omega t$, inserted into the piston position error feedback (4), acts as a harmonic excitation of the nonlinear pitch bearing-blade-actuator system:

$$\dot{\mathbf{x}} = \mathbf{f}\left(\mathbf{x}, t\right) \tag{10}$$

where the state vector is $\mathbf{x} = \{q_e, q_f, q_t, \theta_p, \dot{q}_e, \dot{q}_f, \dot{q}_t, \dot{\theta}_p, P_A, P_B\}^T$, and $\mathbf{f}$ is a nonlinear periodic function $\mathbf{f}(\mathbf{x}, t) = \mathbf{f}(\mathbf{x}, t + T)$ for $\mathbf{x}$ constant, where $T = \frac{2\pi}{\omega}$ is the period of excitation.

One could try to obtain the steady state periodic response of this system by time-integration; however, it may require long simulation time before the transients are damped out. Instead, a finite-difference discretization of the system equations is performed over one period of excitation:

$$\mathbf{x}_{i+1} - \mathbf{x}_i = \frac{h}{2}\left(\mathbf{f}(\mathbf{x}_{i+1}, t_{i+1}) + \mathbf{f}(\mathbf{x}_i, t_i)\right) \quad \text{for} \quad i = 0, 1, 2, \ldots, N-1 \tag{11}$$

where the time step is $h = T/N$, and i denotes the time instance t_i where the eight states are $\mathbf{x}_i$. These $8N$ equations have $8(N+1)$ unknown states. However, the initial conditions $\mathbf{x}_0$ are sought for which the solution of (11) becomes periodic $\mathbf{x}_0 = \mathbf{x}_N$, whereby the number of unknowns is reduced to $8N$ and the system of equations (11) can be solved by Newton-Raphson.

Once, the steady state periodic pitch response is computed, a Fourier transform is performed to extract the amplitude and phase of the harmonic component with the frequency ω. This procedure is repeated for any desired number of frequencies ω to obtain the transfer function in a frequency band. Figure 6 shows the transfer functions from reference to actual pitch below 10 Hz for the undeformed and deformed blade with a reference pitch amplitude of $a = 0.5$ deg. As shown later, both transfer functions seem to have the characteristics of second order filters for this amplitude, except around three frequencies: Around 1 Hz, the transfer function for the deformed blade shows a resonant behavior, which is caused by excitation of the edgewise bending mode (with a natural frequency close to 1 Hz) due to the inertia coupling of edgewise bending and torsion when the blade is bend flapwise in this deformation state at 12 m/s. Around 7 Hz, both transfer functions have increases in the transfer magnitude from reference to actual pitch, which are caused by excitation of the actuator mode with a natural frequency close to 7 Hz (cf. Figure 5). Around 8 Hz, both transfer functions show anti-resonant behaviors, which are caused by excitation of the torsional blade mode with a natural frequency close to 8 Hz.

More details on these behaviors can be obtained from the periodic solutions at different frequencies. Figure 7 shows the periodic solutions for the cylinder pressures (P_A and P_B), reference and actual pitch angles (θ_{ref} and θ_p), and blade tip motions (q_e, q_f, and q_t) of the deformed blade at the excitation frequencies 0.1 Hz and 1 Hz. At the low frequency of 0.1 Hz, the actual pitch angle follows the reference pitch angle closely. The blade responses are small. There are 1 Hz variations on top of the 0.1 Hz variations, especially in the edgewise motion.

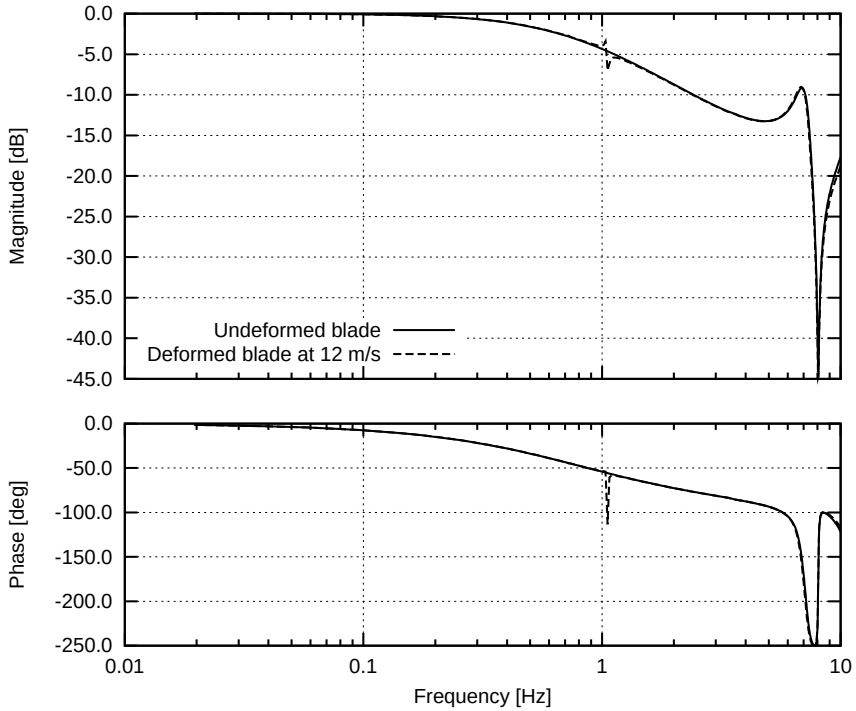

Figure 6. Magnitude and phase of computed transfer functions from reference to actual pitch angles for the undeformed and deformed blade with harmonic reference amplitude of 0.5 deg.

These variations are caused by excitation of the edgewise blade mode due to impulses in the actuator torque that arise when the check valve opens and closes, resulting in time-gradient discontinuities in the B-side pressure as it is limited to the accumulator pressure. The larger impulse during the opening also causes a small excitation of the torsional blade mode.

In the right plots of Figure 7 for the excitation frequency of 1 Hz close to the edgewise natural frequency, there is a significant edgewise component in the blade tip motion due to this near resonant excitation. The periodic solution for the pressures shows that opening and closing of the check valve during one period of oscillation are slightly softer; however, there is a small excitation of the actuator blade mode seen as 7 Hz variations in the A-side pressure and the blade torsional response. The periodic solution for the actual pitch angle confirms the amplitude reduction and phase shift from Figure 6.

Figure 8 shows the periodic solutions for the deformed blade at higher excitation frequencies 7 Hz and 8 Hz. At the frequency of 7 Hz close to the natural frequency of actuator mode (cf. Figure 5), there are significant variations in the cylinder pressures due to the resonant excitation of this mode related to the compressibility of the oil and flexibility of the hoses. This resonant excitation of the actuator mode increases the pitch torque variation at around this frequency. It explains the increased actual pitch angle response seen in Figure 6, but it also causes a large torsional blade response with a blade tip amplitude of 2 deg due to the nearness of the natural frequency of torsional blade mode at 8 Hz. It is noted that the torsional blade motion is in phase with the reference pitch angle and the pressure difference $P_A - P_B$, and thereby the pitch torque, whereas the actual pitch angle is in counter phase with the reference pitch angle.

At the excitation frequency of 8 Hz, there is almost no response in the actual pitch angle, as also seen by the anti-resonance in Figure 6, all excitation energy goes into the torsional blade mode, resulting in a blade tip amplitude of 1 deg. At this high frequency further away from the actuator mode frequency, the B-side pressure is very close to the accumulator pressure, which

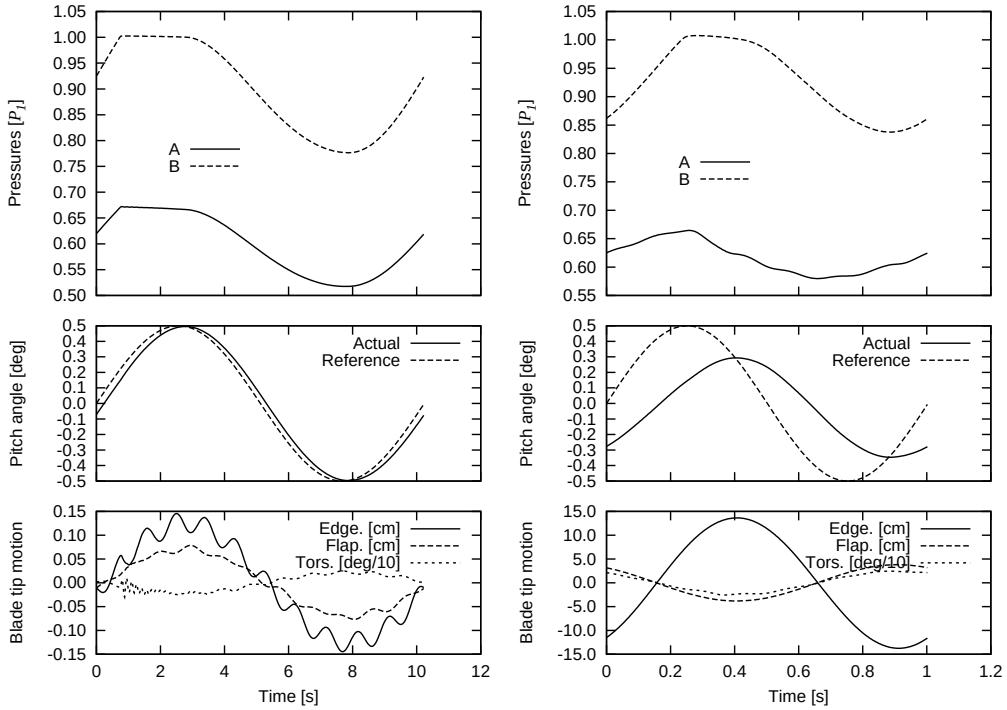

Figure 7. Cylinder pressures (top), reference and actual pitch angles (middle) and relative blade tip motion (bottom) for the deformed blade and excitation frequencies: Left around 0.1 Hz and right around 1 Hz.

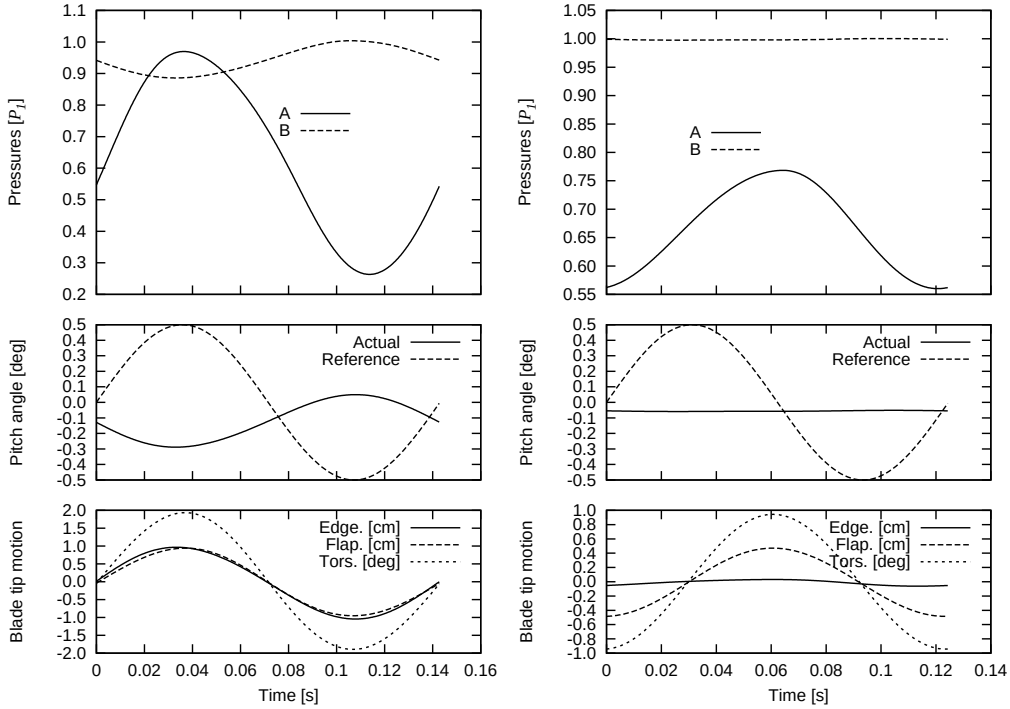

Figure 8. Cylinder pressures (top), reference and actual pitch angles (middle) and relative blade tip motion (bottom) for the deformed blade and excitation frequencies: Left around 7 Hz (actuator frequency) and right around 8 Hz (torsional frequency).

shows that the check valve is almost continuously open. Note that there is a small offset in the actual pitch angle which is caused by the biasing effect of (relative) high-frequency excitation of strongly nonlinear systems [10].

Figure 9 shows the transfer functions from reference to actual pitch angles for the deformed blade when the reference pitch amplitude is changed from 0.01 deg to 5 deg. These functions show the nonlinear effects of the limitations in valve flows, whereas limitation of the maximum torque, and thereby the pitch acceleration, has a minor effect.

The maximum actuator torque can be approximated by $r_p P_1(A_A - A_B)$ and $r_p(P_1 A_B - P_0 A_A)$ for pitching in the two directions, assuming that the viscous forces on the piston can be neglected. If these maximum torques are divided by the rotational pitch inertia I_p, it can be shown that the maximum pitch acceleration of the deformed blade is over 100 deg/s^2. Such high limit indicates that the cylinder may be over-dimensioned. The maximum pitch velocity can be approximated by $Q_{c,max}/A_B/r_p \approx 2$ deg/s and $Q_{p,max}/A_A/r_p \approx 9$ deg/s for pitching in the two directions, where $Q_{c,max} = 50$ l/min and $Q_{p,max} = 300$ l/min are the imposed maximum obtainable flows through the check and proportional valves, respectively. These low maximum limits on pitch velocity show that the two valves with the imposed flow limits are under-dimensioned (especially the check valve) relative to the over-dimensioned cylinder for the given torque arm r_p.

The transfer function in Figure 9 for the pitch reference amplitude of 5 deg is the only function to show significant limitations of the actuator. This limitation of the actual pitch angle starts around 0.1 Hz, which corresponds to a maximum pitch velocity of about 3 deg/s and a maximum acceleration of about 2 deg/s^2. From the theoretical predictions of the maximum pitch velocity and acceleration, it is concluded that the reduction of the transfer function at 5 deg reference pitch amplitude above 0.1 Hz is caused by the under-dimensioned valves (or the over-dimensioned cylinder), setting a low maximum limit on the pitch velocity.

The above results show that the analyzed hydraulic pitch actuator may not be well-designed

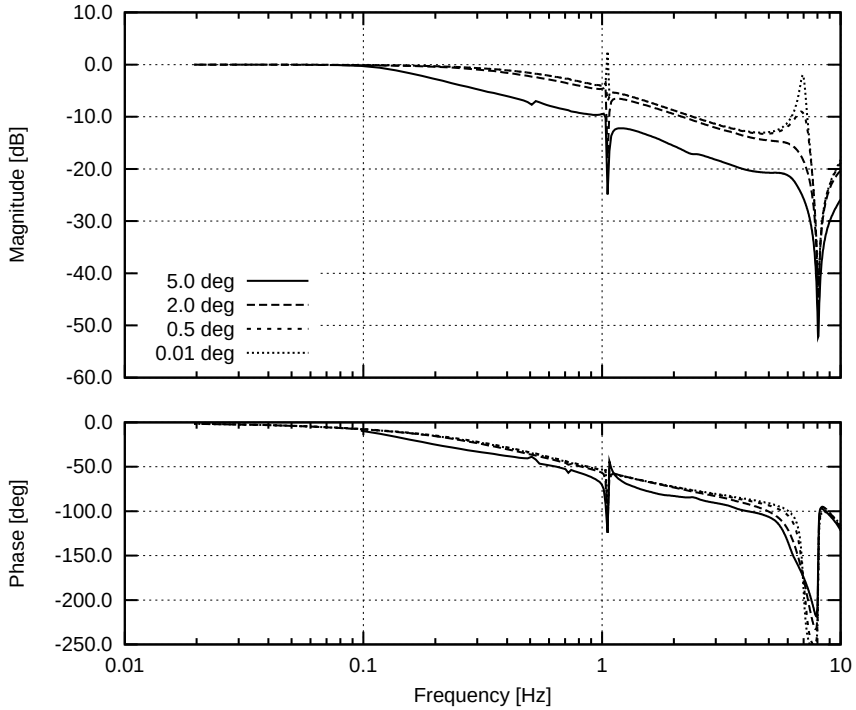

Figure 9. Magnitude and phase of computed transfer functions from reference to actual pitch angles for the deformed blade with different reference amplitudes: 0.01, 0.5, 2 and 5 deg.

for the 5 MW RWT. However, the analysis shows the method for redesigning the actuator with respect to its geometry and the sizes of the valves and the cylinder.

4.1. Second order filter approximation

In aeroelastic simulations of wind turbines, the pitch actuator is often modeled as a second order low-pass filter, i.e., the transfer function from reference and actual pitch angles is approximated by the complex function

$$H_f(\omega) = \frac{\omega_0^2}{\omega_0^2 - \omega^2 + i2\beta\omega_0\omega} \tag{12}$$

where ω_0 and β are the frequency and damping ratio of the second order filter, respectively.

Figure 10 show a fit of this second order filter transfer function to the transfer function for the deformed blade obtained from the physical model with a pitch reference amplitude of 0.5 deg (cf. Figure 6). A good fit is obtained for a filter frequency ω_0 of 10 Hz and a damping ratio β of 6.5. The simple filter model of the actuator based on angles only does not capture the interaction with the blade modes around 1 Hz and 8 Hz, and of course not the hydraulic pitch actuator mode at 7 Hz. Furthermore, the transfer function $H_f(\omega)$ of this linear filter is independent of the pitch reference amplitude. However, it may be possible to model the limitations of the actuator by imposing limitations on the maximum pitch velocity and accelerations.

5. Conclusion

The servo-elastic dynamics of a hydraulic pitch actuator acting on a flapwise bend wind turbine blade is considered in this paper. The actuator is controlled by a proportional feedback of the piston position error to a proportional valve that regulates the flows to the two cylinder sides.

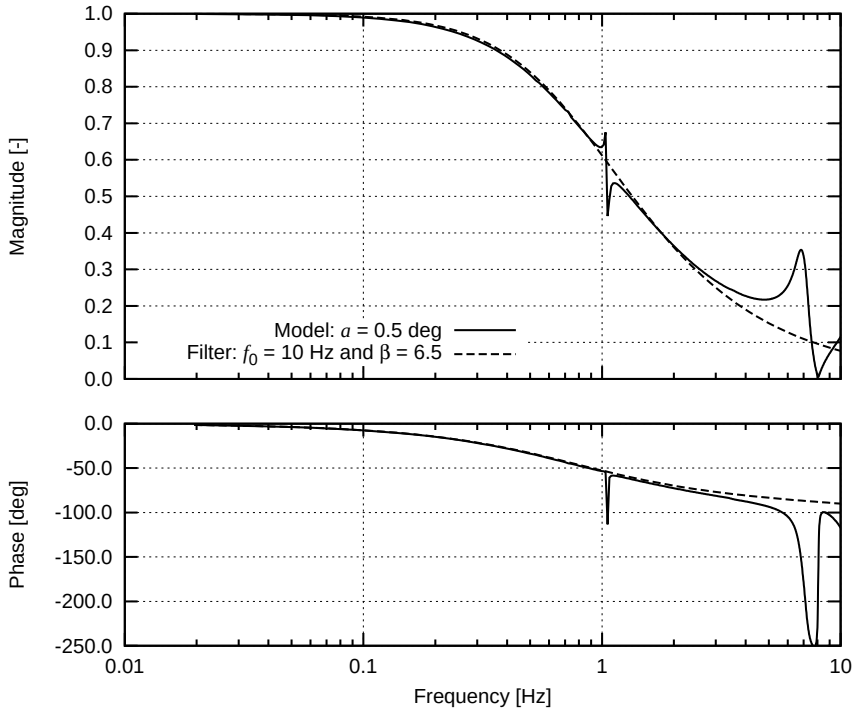

Figure 10. Magnitude and phase of computed and approximated transfer functions from reference to actual pitch angles for the deformed blade with harmonic reference amplitude of 0.5 deg. Second order filter parameters are frequency of 10 Hz and damping ratio of 6.5.

The hydraulic model includes the compressibility of the oil and flexibility of the hoses, causing an actuator mode to arise in the characteristics of the actuator. The structural model of the blade of a 5 MW turbine includes the bending–torsion inertia coupling when the blade is largely bend. The analysis of the blade-actuator dynamics shows that the transfer function from reference to actual pitch angles can be approximated below 10 Hz by a second order low-pass filter, except for frequencies around the natural frequencies of the edgewise bending and torsional blade modes and the actuator mode, where resonant responses are observed. Friction in the pitch bearing is not included in this first analysis. The blade load dependent friction in the pitch bearing may change the presented servo-elastic dynamics of the actuator–blade system towards more complex characteristics due to this highly nonlinear effect.

6. References

[1] J. Jonkman. NREL 5 MW baseline wind turbine. Technical report, NREL/NWTC, 1617 Cole Boulevard; Golden, CO 80401-3393, USA, 2005.
[2] P. Caselitz, M. Geyler, J. Giebhard, and B. Panahandeh. Hardware-in-the-loop development and testing of new pitch control algorithms. In *Scientific Proceedings of the European Wind Energy Conference 2006*, pages 60–64, Athens, Greece, 2006.
[3] T. J. Larsen, A. M. Hansen, and T. Buhl. Aeroelastic effects of large blade deflections for wind turbines. In *Proceedings of The Science of Making Torque from Wind*, pages 238–246, The Netherlands, April 2004. Delft University of Technology.
[4] A. Ahlström. Influence of wind turbine flexibility on loads and power production. *Wind Energy*, 9:237–249, 2006.
[5] M. H. Hansen and T. Buhl. Design guidelines for passive instability suppression – Task-11 Report. Technical Report Risø–R–1575(EN), Risø National Laboratory, Denmark, December 2006. (Available from www.risoe.dk).
[6] B. S. Kallesøe. Equations of motion for a rotor blade, including gravity, pitch action and rotor speed variations. *Wind Energy*, 10:209–230, 2007.
[7] B. S. Kallesøe. Large blade deformations effect on flutter boundaries. In C. Bak, editor, *Research in Aeroelasticity, EFP-2006*, number Risø-R-1611(EN). Risø National Laboratory, Technical University of Denmark, Roskilde, Denmark, June 2007. (To appear on www.risoe.dk).
[8] R. W. Clough and J. Penzien. *Dynamics of Structures*. McGraw-Hill, 1975.
[9] A. H. Nayfeh and B. Balachandran. *Applied Nonlinear Dynamics*. Wiley, 1995.
[10] J. J. Thomsen. *Vibrations and Stability*. Springer Verlag, 2003.